J. Comp. App. Res. Mech. Eng. Vol. 14. No. 1, pp. 129-141, 2024 *DOI: 10.22061/jcarme.2024.10461.2377*

Journal of Computational and Applied Research in Mechanical Engineering
jcarme.sru.ac.ir
SRTTU
JCARME
ISSN: 2228-7922

Research paper

The effect of Cu concentration on tensile and compression properties of Ti-10Mo alloy using molecular dynamics simulations

Aji Abdillah Kharisma[a], Haris Rudianto[a, *], Achmad Benny Mutiara[b] and Sulistyo Puspitodjati[b]

[a]*Department of Mechanical Engineering, Gunadarma University, Depok, West Java, 16431, Indonesia*
[b]*Department of Information Technology, Gunadarma University, Depok, West Java, 16431, Indonesia*

Article info:

Article history:

Received:	15/11/2023
Revised:	05/09/2024
Accepted:	07/09/2024
Online:	09/09/2024

Keywords:
TiMoCu alloys,
Compression loading,
Tensile loading,
MD simulations,
Structure evolution.

[*]Corresponding author:
harisrudianto@staff.gunadarma.ac.id

Abstract

Titanium alloys have been extensively explored and fabricated for application in several engineering fields. Its superior mechanical properties, Ti-10Mo-xCu alloy has potential applications in hip implants. Determining mechanical qualities via experimental methods takes a long time, especially in compression and tensile testing. Therefore, material design modeling using an MD simulation method approach is used to evaluate the mechanical properties of the compression and tensile tests of the Ti-10Mo-xCu alloy. In this research, material design through computer modeling is carried out at 300 K in the x <100> direction of the Ti-10Mo alloy with the addition of Cu composition at 3, 6, and 9 wt.% to evaluate the properties of the alloy. The simulation results of the Cu addition produce maximum stresses of 603, 160, and 236 Mpa, respectively. The experimental method in the compression test shows a decrease in the maximum stress after adding Cu to the Ti-10Mo alloy. It has the same trend value as the compression test outcomes on the experiment and MD simulation method. The tensile strength results for the Ti-10Mo-xCu alloy are 7056.8, 7238.2, and 7433.1 Mpa, respectively. MD simulation of the results of crack propagation in tensile strength is successfully performed based on the increase at high strain until plasticity occurs in the alloy.

1. Introduction

For a long time, materials science study has become more popular due to the mechanical properties of metals [1, 2]. A hip fracture is a failure in the upper thighbone. Elderly patients are most commonly affected by hip fractures. When a hip fracture develops in a younger patient, it is frequently the result of a high-energy activity. Hip implants are usually made of titanium alloys [3] due to their excellent mechanical qualities, such as tensile and compressive strength [4]. Testing the mechanical properties of hip implants using experimental methods is required for a very long time in the process, especially for testing the mechanical properties of compression tests. Therefore, it is necessary to carry out material design modeling using the molecular dynamic

simulation method approach, which can evaluate to obtain faster results from the compression test. The computational method provides a solution for material handling under extreme conditions in the laboratory, such as high temperature and pressure [5]. In 1960, Gibson and Vineyard used MD simulations to investigate radiation damage in Cu [6]. In 1964, Rehman [7] used MD simulations to simulate atomic motion in the liquid argon. In 1967, Verlet [8] solved the classical principles for movement between atoms by implementing the Verlet integration.

Additionally, research on the molecular dynamics simulations of the Cu/W interface shows higher [1 1 0] and [1 1 2] copper yield points and substantially reduced strengths of [1 1 1] copper [9]. Recent investigation, using 2NN MEAM, showed acceptable interatomics for structures Mn-Ni, Co-Fe, Cr-Mn, and Co-Cr are constructed [10]. Diffusion bonding at the Mo-Ti interface is critical for bonding composite structures via the temperature effect in MD simulations. When the Ti composition exceeds 50%, the HCP structure is shown to be more stable than the BCC structure [11]. The potential of (Ti1) forming the HCP-BCC transformation to simulate plasticity damage on the HCP Ti property target α (HCP) (Å) is 2.951 [12].

On the other hand, the researchers released various studies on structural aspects, phase transition, crystal growth process, mechanical and magnetic properties on the alloys (such as Cu-Ti [13], Bulk Cu [14], Cubic Cu–Au [15-17], $Ag_{1-x}Au_x$ NiAu, and $Fe_{1-x-y}Ni_xCo_y$ alloys [18-20], when the concentration of Cu increases, the proportion of the crystal structure system changes. Recently, many studies on Ti-based alloys made of various materials have been released via molecular dynamic simulation especially mechanical properties such as compression and tensile test, structural change transformation, such as Cu/W, Mo/Ti interfaces, [9, 11], Ti-9Mo and Ti-10Mo alloys [21, 22], TiAl alloy, γ-titanium aluminide, TiNi alloy, (TiAl)/α_2(Ti_3Al) [23-26], single crystal Al [27], TiV alloys [28], copper nanowire [29], Ti-Cu alloy [30]. Nevertheless, as closely as the authors are mindful, no previous research describes the mechanical behavior and structure evolution of Ti-10Mo alloys with the addition of 3Cu, 6Cu, and 9Cu at the atomic scale under uniaxial tensile and compression loading. The outcome of the present research is to model the material design of Ti-10Mo-xCu alloys using the results of compression test. The result is compared with MD simulation and experimental techniques. Tensile test modeling with MD simulation is used to forecast stress-strain findings and structural deformation changes that occur without comparing them to experimental results.

2. Computational procedure

2.1. Interatomic potentials

The modified embedded atom model (MEAM), provided by M.I. Mendelev [12], was adopted to simulate. MEAM defines the asymmetry of the shear variable and the departure of the c/a lattice parameter ratio from the most suitable value while retaining a linear function. The c/a lattice parameter ratio from suitable value is 1.587, and lattice parameter a = 2.951 on the Ti-Mo lattice that was refined by referring to earlier results from experiments by B.J. Lee [31]. The interatomic potential applied in the Ti-10Mo-xCu alloy is the modified embedded atom method (MEAM) to define various types of crystal structures such as (FCC, BCC, and HCP) among the atoms [23, 31]. The molecular dynamics simulation system employs classical Newtonian laws of motion.

MD simulations containing N particles with the proper positions and momentum vector were denoted by $r_i = (x_i, y_i, z_i)$ and $p_i = (p_{i,x}, p_{i,y}, p_{i,z})$. The Hamiltonian (H) of the system [32] is expressed with Eq. (1).

$$H\left(R^N, P^N\right) = \sum_{i}^{N} \sum_{\alpha} \frac{p_i^{2,\alpha}}{2m_i} + U\left(R^N\right) \quad (1)$$

here, $R^N = \{r_1, r_2, \ldots, r_N\}$ and $P^N = \{p_1, p_2, \ldots p_N\}$ express the initial spatial coordinates and moment forces of all particles, respectively, U is the potential energy, and the symbol α denotes the three directions (x, y, z), while m_i specifies the mass of the *i* particle.

The energy of the systems moves each particle in response to applied forces. The force with the negative indicates the gradient with Eq. (2). Newton's second Law [32] describes the movement of a particle with Eq. (3).

$$F_i\left(R^N\right) = -\frac{\partial U\left(R^N\right)}{\partial r_i} \quad (2)$$

$$m_i\ddot{r}_i = F_i(R^N) \quad (3)$$

where F_i is the system energy, $\ddot{r}_i$ is the second-order derivative of r_i with relation to time, R^N is the initial location, and P^N is the force moment of the particle against time. The total energy (E_{tot}) in the system is made of the total potential energy (E_p) and kinetic energy (E_k) [33], the formula can be obtained as Eqs. (4 and 5).

$$E_{tot} = E_k + E_p \quad (4)$$

$$E_k = \frac{3}{2} \times N \times k \times T \quad (5)$$

where, E_T expresses the total energy of the atom group, E_p is the total potential energy of the atom group, E_k is the total kinetic energy. k is Boltzmann's constant, N is the number of atoms, and T is the temperature of the system.
The potential energy that occurs between atoms in an atomic crystal lattice system is known as interatomic potential. In the MEAM, the total energy (E) is expressed by Eq. (6).

$$E = \sum_{i}^{N} \left[F(\bar{\rho}_i) + \frac{1}{2} \sum_{j \neq i} \phi_{ij}(r_{ij}) \right] \quad (6)$$

In Eq. (6), F is the embedding energy function, $\bar{\rho}_i$ is the electron density at the location inhabited by the atom i, and ϕ is the interaction among atoms i and j at a distance of r_{ij}.

2.2. Simulation details

In this work, LAMMPS (Large-scale Atomic/Molecular Massively Parallel Simulator) code, was used for materials modeling of Ti-10Mo-xCu alloys related to mechanical characteristics of the compression and tensile test which can be evaluated through OVITO software [34, 35]. In Fig. 1, the initial configuration of modeling is shown. The lattice constant units were built using periodic boundary conditions type is p p p. The system contains 108000 atoms. The system was set up for equilibrium at room temperature during a 10 ps isothermal-isobaric (NPT) ensemble [36, 37]. The pressure is in (zero pressure) for units of metal before conducting a tensile and compression force in the x-direction <100> [38, 39]. Ackland Jones Analysis was used to identify the structural transformations and (CSP) centrosymmetric parameter [40, 41] to identify the local crystalline structure of atoms. MD simulations were carried out at 300 K on compression and tension force [39]. The uniaxial deformation quantities of stress are to be calculated using Eq. (7).
Based on the existing problem statement, shown in Fig. 2, the simulation model results will be validated and verified in order to compare with experimental results.

$$\sigma = \frac{F}{A} \quad (7)$$

The sample dimensions after the compression test are shown in Fig. 3.

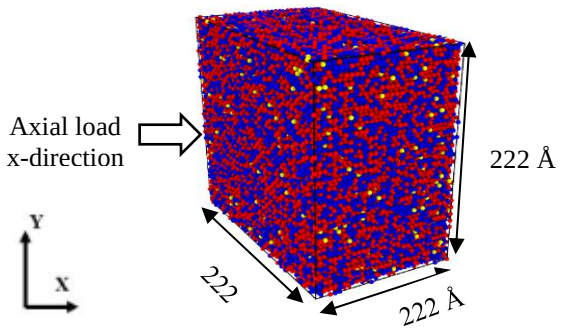

Fig. 1. Initial configuration of modeling. Red, blue, and yellow represent titanium, molybdenum, and copper atoms, respectively.

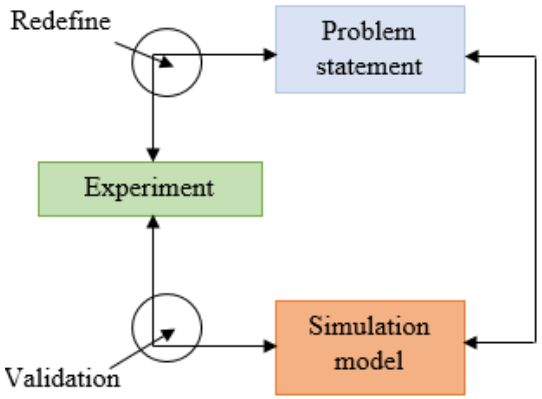

Fig. 2. Stages of the research.

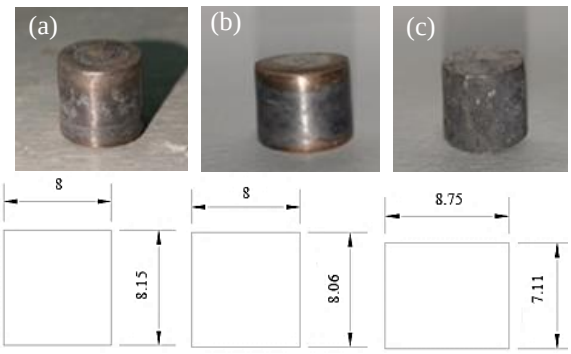

Fig. 3. Dimensions of the samples after compression test; (a) Ti-10Mo-3Cu, (b) Ti-10Mo-6Cu, and (c) Ti-10Mo-9Cu, respectively.

3. Results and discussion

3.1. Stress – strain relation of compression and tensile loading test

In general, stress-strain relationship curves are used to demonstrate that a material performs under loading situations. The modulus of elasticity on the maximum compression and tensile qualities of the material can be calculated using the correlation graph of stress and strain [42, 43]. Fig. 4(a) shows, in the <100> x-direction, the result of the stress-strain graph for the compression testing on the Ti-10Mo-3Cu alloy, proving a significantly higher peak stress at 300 K compared to those of the Ti-10Mo-6Cu and Ti-10Mo-9Cu, as represent in Fig. 4(b and c). Table. 1 provides the extracted mechanical properties of the compression tests. It indicates that the stress and strain values of the Ti-10Mo-xCu alloy containing 3, 6, and 9 wt.% Cu are 603, 160, and 236 MPa, and 0.153, 0.240, and 0.189, respectively. It can be seen that increasing the Cu amount decreases the stress values. Moreover, the values of modulus elasticity in the x-direction of compression loading are 4020, 816, and 967 MPa, respectively(see Table. 1). This finding is similar to the prior experiment results [24] and [44, 45] which revealed that when the percentage of Cu addition increases can produce the modulus of elasticity decreases. The maximum stress values of the Ti-10Mo-3Cu, Ti-10Mo-6Cu, and Ti-10Mo-9Cu alloys are 7056.8, 7238.2, and 7433.1 MPa, respectively, with the strain values of 0.355, 0.356 and 0.377, as shown in Fig. 5. The highest stress corresponds to the maximal force during stretching that a material meets when strained before breaking. The increase in the copper percentage can improve the mechanical quality of the Ti-10Mo-xCu alloys for use as a hip implant [46-49]. The results have the same trend as reported by Xu et al. [46]; the yield strength of the Ti-14Cu alloy increased by 30%, and UTS increased by 25% with the addition of Cu element.

3.2. Number of structural type units

Fig. 6(a, b, and c) shows the number of structural units for Ti-10Mo-xCu alloys in the compression test with four structural types of crystal: HCP (hexagonal close-packed), orange, FCC (face-centered cubic), and gray (amorphous). Ti-10Mo-6Cu alloys produced 8991 FCC, 54347 HCP, 9029 BCC, and Amor 33362. Those of Ti-10Mo-9Cu are 9317 FCC, 56105 HCP, 9192 BCC, and 34887 Amor.

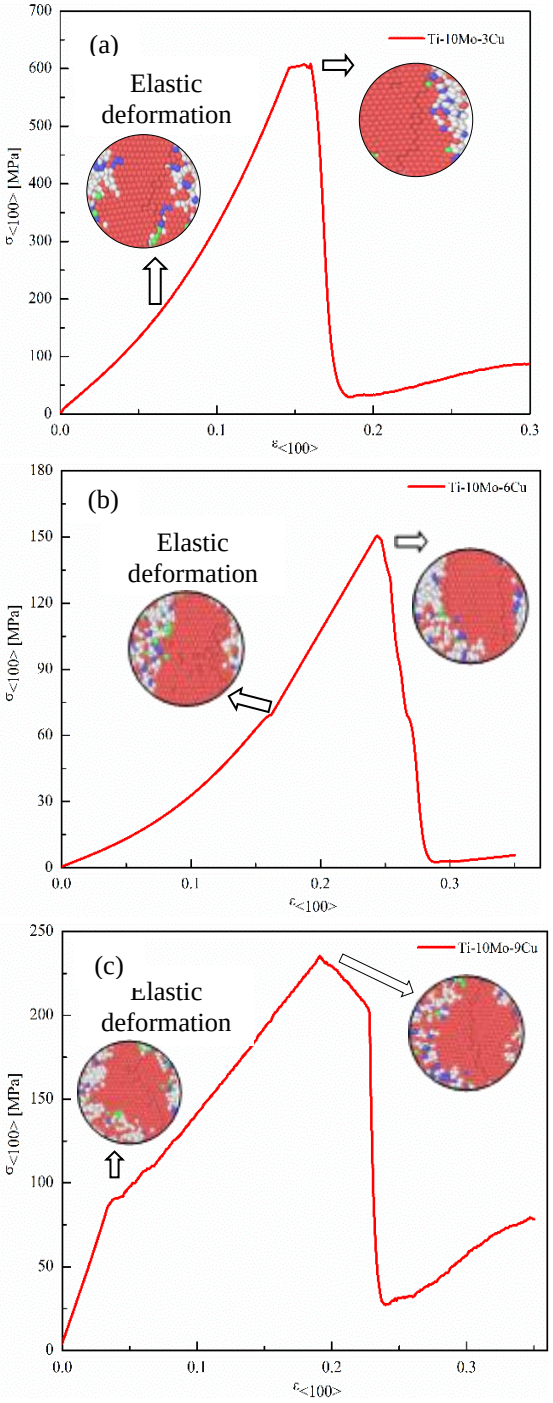

Fig. 4. Engineering stress-strain curve for compression tests of titanium alloys with x-direction <100> (a) 3, (b) 6, and (c) 9 wt.% Cu, respectively.

Table. 1. The results of compression test.

Properties	Alloy	σ_{max} (MPa)	ε	E (MPa)
Compression	Ti-10Mo-3Cu	603	0.153	4020
	Ti-10Mo-6Cu	160	0.240	812
	Ti-10Mo-9Cu	236	0.189	967

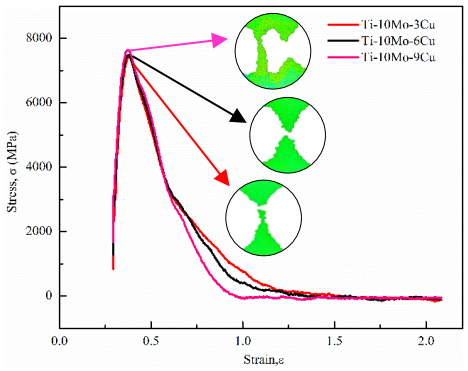

Fig. 5. Stress-strain curves of titanium alloys in tensile test with MD simulation.

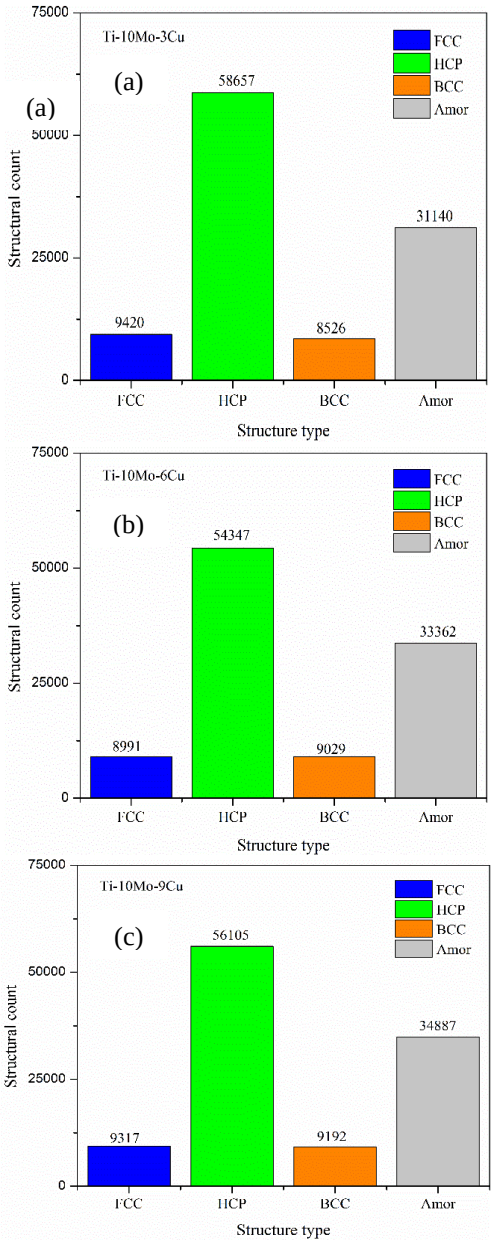

Fig. 6. Number of structural type units for Ti-10Mo alloy; (a) 3Cu, (b) 6Cu, and (c) 9Cu of compression test, respectively.

Fig. 7(a, b, and c) shows the number of structural units in the Ti-10Mo-xCu alloys in the tensile test. Ti-10Mo-3Cu has 1664 FCC, 104365 HCP, 1403 BCC, and Amor 15111. Ti-10Mo-6Cu shows 3528 FCC, 77380 HCP, 8930 BCC, and Amor 31274. Ti-10Mo-9Cu has 3386 FCC, 77134 HCP, 8559 BCC, and Amor 32218. The number of lattices is unchanged as the strain rate decreases. This is inversely proportional, the fast deformation can generate more HCP lattice structural change [50]. This is consistent with the present simulation results, which are presented in Figs. 6 and 7.

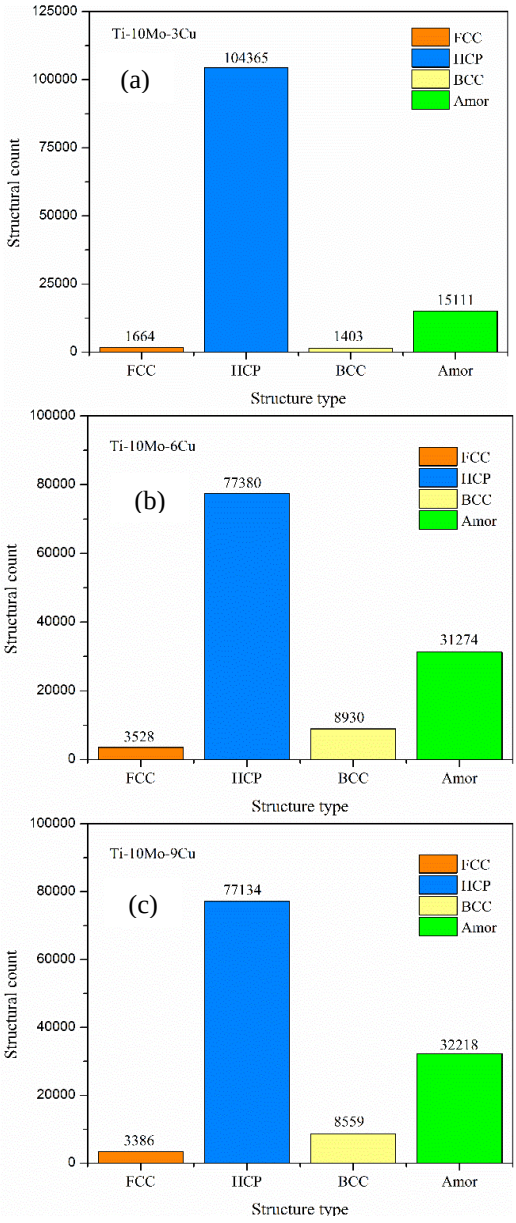

Fig. 7. Number of structural type units for Ti-10Mo alloys; (a) 3Cu, (b) 6Cu, and (c) 9Cu of tensile test, respectively.

The HCP structure number grows as the strain increases. In Figs. 6 and 7, the highest HCP structure type counts for tensile and compression are 104365 and 58657 on the Ti-10Mo-3Cu, respectively, indicating that the tensile test has the same condition as that of the compression test when strain increases.

According to the structure type count of the HCP displayed in Fig. 7, these results have suitable similarities, where the quantity of HCP structure in the compression test result is substantial, namely with the addition of 3, 6, and 9 wt% Cu in the Ti-10Mo alloy in the compression test at the end of the simulation. Fig. 7(a, b, and c) shows the number of structural units in the Ti-10Mo-xCu alloys in the tensile test. Ti-10Mo-3Cu has 1664 FCC, 104365 HCP, 1403 BCC, and Amor 15111. Ti-10Mo-6Cu shows 3528 FCC, 77380 HCP, 8930 BCC, and Amor 31274. Ti-10Mo-9Cu has 3386 FCC, 77134 HCP, 8559 BCC, and Amor 32218. The HCP (hexagonal closed package) transforms into an amorphous, BCC, and a small quantity of FCC structure type [50]. This is consistent with the present simulation results, which are presented in Figs. 6 and 7. The HCP structure number grows as the strain increases. In Figs. 6 and 7, the highest HCP structure type counts for tensile and compression are 104365 and 58657 on the Ti-10Mo-3Cu, respectively, indicating that the tensile test has the same condition as that of the compression test when strain increases.

According to the structure type count of the HCP displayed in Fig. 7, these results have suitable similarities, where the quantity of HCP structure in the compression test result is substantial, namely with the addition of 3, 6, and 9 wt.% Cu to the Ti-10Mo alloy in the compression test at the end of the simulation.

3.3. Illustration of structural evolution

In Fig. 8, the centrosymmetric parameter is an important indicator for identifying localized lattice disordered surrounding an atom in a solid-state structure. It is implemented to determine when the particles are considered to be bonded by a similar lattice [30]. Red atoms are classified as being in centrosymmetric circumstances, whereas in the simulation box, particles of different colors are classified as being in a non-centrosymmetric condition, implying that a dislocation happened in the atomic structure. The illustration of the respective atomic dislocation mechanisms that occur in Fig. 8(a) displays strain values of 0.074 and 0.153. The strain value is very significant when compared to the dislocations that were found in the modeling results, as illustrated in Fig. 8(b and c).

Fig. 9 represents a snapshot of the atomic configuration with a stress tensor in the x-direction, showing the tensile deformation that develops in the Ti-10Mo-xCu alloy at 300 K. Fig. 9(a) shows the regularly organized atoms before relaxing in a state without any pressure applied on the Ti-10Mo-xCu alloy. During the tensile test, several initial dislocations (red arrows in Fig. 9(b) started moving to the boundaries and stacking to that location, caused by the high energy of grain boundaries [51]. The considerable differences in grain boundary structures were noticed following peak loading. This phenomenon was caused by more frequent grain boundary slips at high strain values [52] with strain values of 0.298, 0.310, and 0.259 on the Ti-10Mo-xCu alloys (see Fig. 9(c)). As a result, the initial dislocation moves away from the free surface and propagates until it reaches a slip stage. Referring to the curves illustrated in Fig. 5, the plasticity-deformed mechanism occurs continuously with increasing strain value.

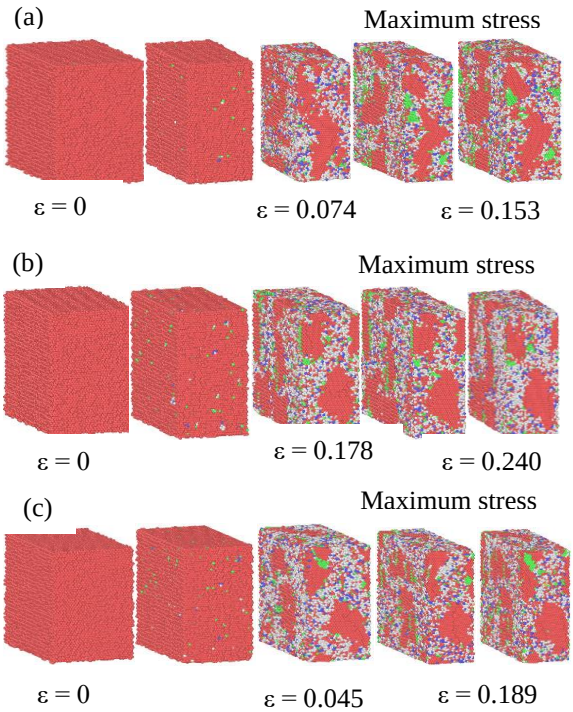

Fig. 8. Atom configuration for uniaxial compression loading with centrosymmetric of Ti-10Mo alloy; (a) 3Cu, (b) 6Cu, and (c) 9Cu in the <100> direction, respectively.

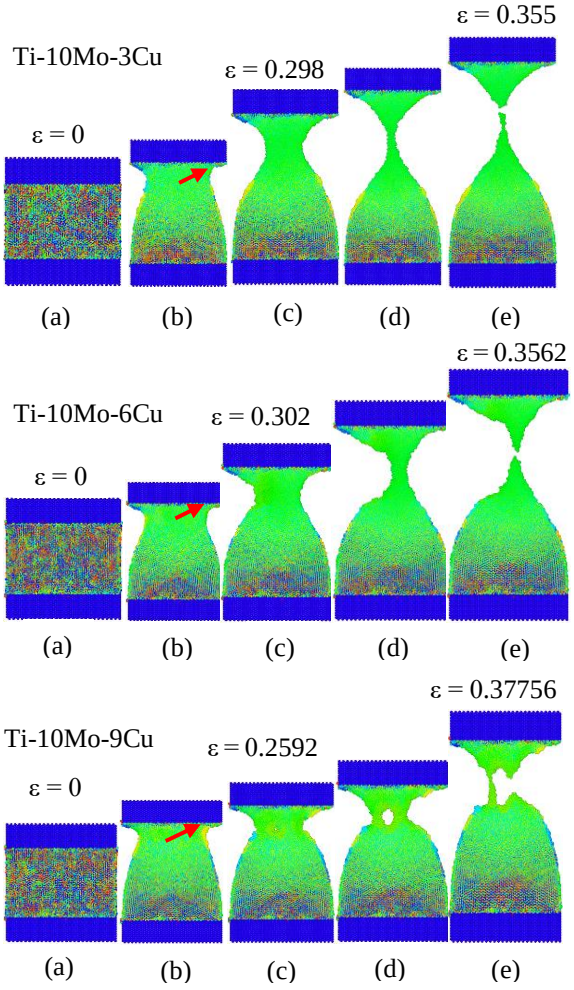

Fig. 9. Illustration of atomic configurations of titanium alloys with color coding during 300 K; (a) regularly organized atoms, (b) initial dislocations, (c) grain boundary slip, (d) atomic neck, and (e) plastic deformation of tensile test

Fig. 9(d) illustrates the atomic necks found in the Ti-10Mo-xCu alloy structure due to the pressure load which, continues to increase towards the ultimate strength of the atom structure. Ultimately, the plastic deformation is generated with occurring shearing crack on the neck in the atomic structure of Ti-10Mo-xCu alloys, as illustrated in Fig. 9(e) with strain values of 0.355, 0.3562, and 0.37756 on the Ti-10Mo alloys with the addition of 3, 6, and 9 wt.% Cu, respectively.

3.4. Radial distribution function of titanium alloys

The RDF of Ti-10Mo-xCu alloy during compression and tensile stress are shown in Figs. 10 and 11 in the <100> direction.

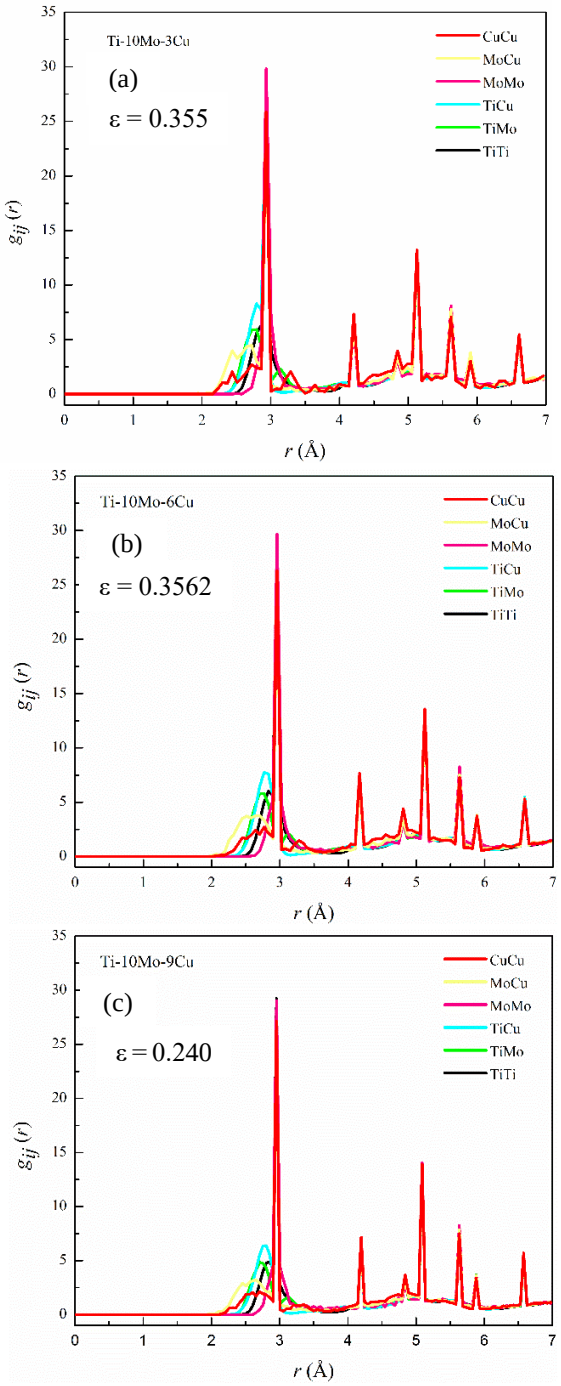

Fig. 10. Partial rdf g_{ij} for tensile; (a) 3Cu, (b) 6Cu, and (c) 9Cu on titanium alloy in the x-direction, with black, purple, yellow, green, blue, and red lines depicted of the TiTi, MoMo, MoCu, TiMo, TiCu, and CuCu pairs, respectively.

Fig. 10(a and b) displays the Ti-10Mo-3Cu and Ti-10Mo-6Cu have the sharpest peaks in the MoMo pair at the moment of tensile loading, with strain values of 0.355 and 0.362, respectively (at maximum stress), and the highest peak in Fig. 10(c).

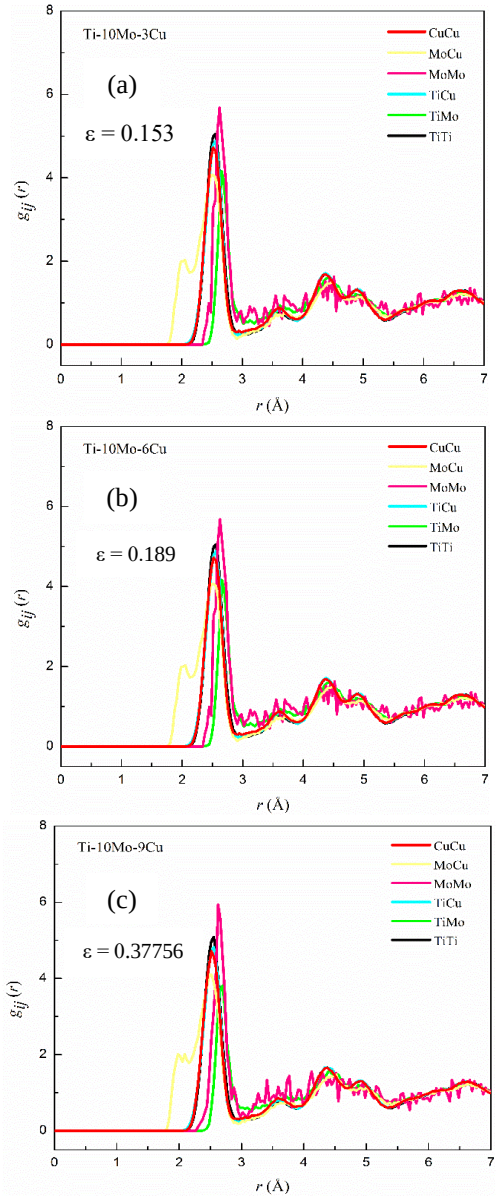

Fig. 11. Partial rdf g_{ij} for compression; (a) 3Cu, (b) 6Cu, and (c) 9Cu on titanium alloy in the x-direction, with black, green, blue, purple, yellow, and, red lines depicted of the TiTi, TiMo, TiCu, MoMo, MoCu, and CuCu pairs, respectively.

9Cu is discovered at the TiTi pair having a strain of 0.37756 (at ultimate strength). The sharpest peaks in Figs. 10 and 11 demonstrate that the Ti, Mo, and Cu atom pairs have strong and constant bonding contacts with the surface on the uniaxial tensile and compression loading. The result that follows was made because the Ti, Mo, and Cu atoms were in separate regions, consequently, the distance between them extended under a tensile force.

The data found reveal that as the timestep increases corresponding with the pressure, E_{tot} always increases continuously. Cu is a conductive metal with excellent thermal properties. The effect of Cu doping on the titanium alloy can provide optimal electrical properties. Copper doping can reduce the surface area and band gap energy of titanium [53]. The obtained results show that when timestep increases from 0 to 17000 for all Ti-10Mo-xCu alloys in the compression test, the E_{tot} increases from E_{tot} = 0 eV to E_{tot} Ti-10Mo-3Cu, 6Cu, and 9Cu = −2550, -2570, and 2580 eV, respectively. The rij and gij(r) from all values of rTi-Mo, rTi-Cu, and rMo-Cu has produced an increase on the Ti-10Mo-xCu alloy compression and tensile tests (see Tables 2(a, b) and 3(a, b)).

The relationship between the E_{tot} and timestep is shown in Fig. 12. In the tensile test, the E_{tot} increases from E_{tot}= 0 eV to E_{tot}Ti-10Mo-3Cu,6Cu, and 9Cu = −1466, -1466.75, and -1467 eV, respectively, as shown in Fig. 13. The influence of pressure (loading) parameters is determined by the electronic structure, such as conductivity and resistivity.

Table. 2(a) Length of links (r, Å) for Ti-10Mo-xCu alloy of the compression test.

Element	r_{Ti-Ti}	r_{Ti-Mo}	r_{Ti-Cu}	r_{Mo-Cu}
Ti-10Mo-3Cu	2.6	2.7	2.68	2.55
Ti-10Mo-6Cu	2.59	2.72	2.75	2.6
Ti-10Mo-9Cu	2.73	2.83	2.77	2.62

Table. 2(b) Height peak g(r) for Ti-10Mo-xCu alloy of the compression test.

Element	Ti-Ti	Ti-Mo	Ti-Cu	Mo-Cu
Ti-10Mo-3Cu	5.08	4.12	3.97	4.1
Ti-10Mo-6Cu	5.15	4.27	4.35	4.2
Ti-10Mo-9Cu	5.25	3.97	4.50	4.35

Table. 3(a) Length of links (r,Å) for Ti-10Mo-xCu alloy of the tensile test.

Element	r_{Ti-Ti}	r_{Ti-Mo}	r_{Ti-Cu}	r_{Mo-Cu}
Ti-10Mo-3Cu	28.5	25.7	26.6	25
Ti-10Mo-6Cu	29.5	26.2	27.5	25.4
Ti-10Mo-9Cu	29.9	27.3	27.7	26.5

Table. 3(b) Height peak g(r) for Ti-10Mo-xCu alloy of the tensile test.

Element	Ti-Ti	Ti-Mo	Ti-Cu	Mo-Cu
Ti-10Mo-3Cu	5.0	4.03	4.8	3.9
Ti-10Mo-6Cu	5.12	4.17	4.95	3.96
Ti-10Mo-9Cu	5.20	4.0	5.15	4.14

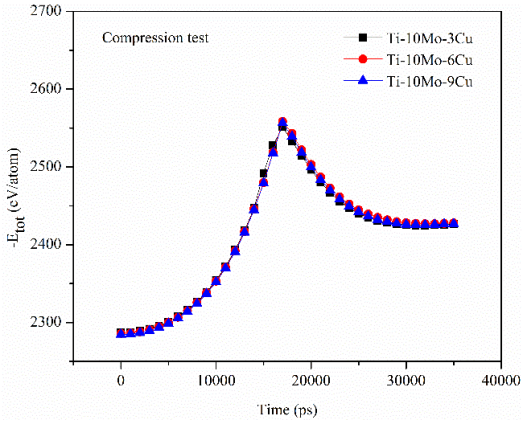

Fig. 12. Atomic potential energy vs timestep graph under different Ti-10Mo-xCu alloys of compression test.

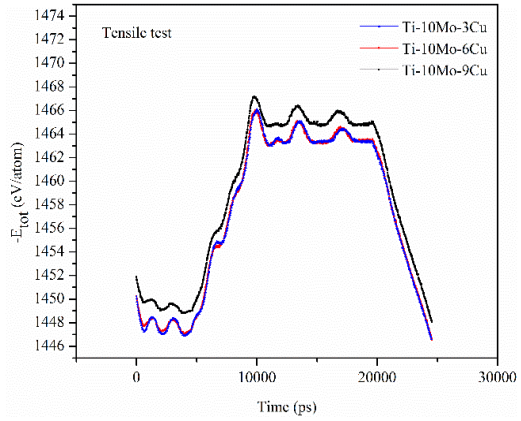

Fig. 13. Atomic potential energy vs timestep graph under different Ti-10Mo-xCu alloys of tensile test.

The density or volume of the alloy decreases as the pressure increases with the time step. It can increase the electrical resistance value and generate superior electronic properties [54, 55].

3.5. Validation of the titanium alloys modeling between simulation and experiment method

The validation of the Ti-10Mo-xCu design model in the compression test is shown in Fig. 14. The size of lattice length of HCP in the simulation model is 220 Å. In HCP, c and a are 0.460 and 0.282 nm, respectively [56]. The size of the simulation box on the simulation model of the compression test is (30 × 30 × 30). The value lattice length from the calculation is:

c = 0.460 nm × 30 = 13.8 nm = 138 Å
a = 0.280 nm x 30 = 8.4 nm = 84 Å.

The total lattice length (c+a) is 222 Å. The volume of the titanium alloy of the MD simulation model must be determined in order to compare the results with the sample size used in the experiment for generating validation output. The volume of HCP can be calculated as:

a = 2r, so finding the value of, $r = \frac{a}{2}$

$r = \frac{0.88\ mm}{2} = 0.44$ mm, so a = 2 × 0.44 mm= 0.88 mm and c is 1.633 × a = 1.633 × 0.88 mm = 1.437 mm. The value of volume HCP Ti alloys is 9.8 mm and can be calculated as shown in Eq. (8).

$$\text{Volume HCP} = 6 \times \frac{a^2\sqrt{3}}{4} \times C \quad (8)$$

Fig. 14(a) shows the result of the MD simulation model, to adjust in Fig. 14(b) the experimental sample. The compression test sample size used in the experimental method is 10 mm and the HCP volume in Ti alloy is 9.8 mm very close to the size value from the other. From Fig. 14, the molecular dynamic simulation generates a lower value, which is consistent with the experimental results [16]. Fig. 15 shows the effect of the addition of Cu element which decreases the maximum stress on the MD simulation and experimental method on the compression test. The maximum stress decreases from 603 to 160 MPa in alloys with 3Cu and 6Cu. The stress on 9Cu increases from 160 to 236 MPa.

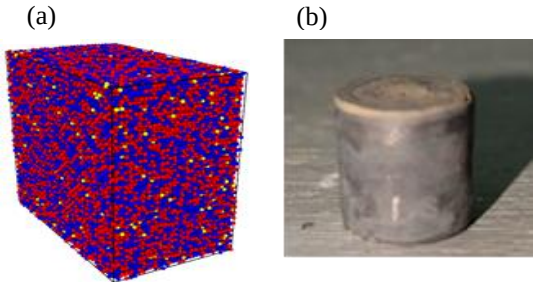

Fig. 14. (a) MD simulation model and (b) experimental sample.

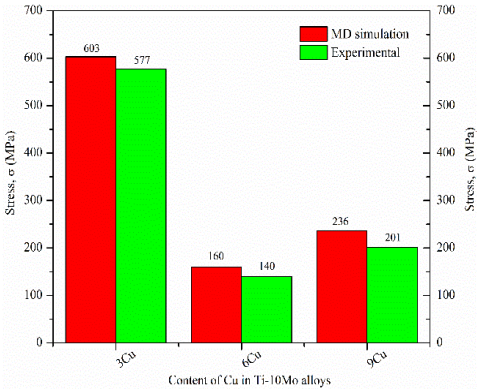

Fig. 15. Comparison of compression test stress values results in experimental and simulation in Ti alloys.

4. Conclusions

In this study, the effects of Cu doping on the composition, crystal structure, and mechanical properties of Ti-10Mo-xCu were investigated by MD simulation on the compression and tensile test. The main conclusions are drawn as follows:

1. The maximum stress value of Ti-10Mo-3Cu, Ti-10Mo-6Cu, and Ti-10Mo-9Cu alloy on the compression test is 603, 160, and 236 MPa, respectively. The highest stress value of 603 MPa occurs on the Ti-10Mo-3Cu alloy. The effect of the addition of Cu element decreases a maximum stress on the MD simulation and experimental method.
2. On the tensile test results, the stress values at Ti-10Mo alloys with 3, 6, and 9wt.% of Cu are 7056.8, 7238.2, and 7433.1 MPa, respectively, with strain values of 0.355, 0.356, and 0.377. The highest stress value of 7433.1 MPa occurs on the Ti-10Mo-9Cu alloy.
3. Molecular dynamics simulation reveals that Ti-10Mo-xCu alloys with cracks rapidly lose stability when subjected to compression and tensile loads. The crack propagation results in the MD compression and tensile simulation are successfully performed based on the increase at high strain with the resulting structural change, the number of structural units, and mechanical deformation.

Conflict of interest

The authors declare no conflict of interest.

Author Contributions

A.A.K., A.B.M., H.R., S.P conceived of the presented idea. A.A.K developed the conceptualization, modeling and performed the computations. A.B.M., H.R., S.P verified the analytical methods and investigated a specific aspect, and supervised the findings of this work. All authors discussed the results and contributed to the final manuscript.

Data Availability Statement

The data that supports the findings of this study are available from the corresponding author upon reasonable request.

Acknowledgment

This work was supported by Gunadarma University, Department of Mechanical Engineering and Information Technology.

References

[1] X. Li, L. Lu, X. Zhang and H. Gao, "Mechanical properties and deformation mechanisms of gradient nanostructured metals and alloys", *Nat Rev Mater.*, Vol. 5, No. 9, pp. 706-723, (2020).

[2] T. O. Olugbade and J. Lu, "Literature review on the mechanical properties of materials after surface mechanical attrition treatment (SMAT)", *NMS.*, Vol. 2, No. 1, pp. 3-31, (2020).

[3] D. F. Williams, "Definitions in biomaterial", *J. Polym. Sci., Part C:Polym. Lett.*, Vol. 26, No. 9, pp. 414-414, (1988).

[4] M. Saini, Y. Singh, P. Arora, V. Arora and K. Jain, "Implant biomaterials: A comprehensive review"., *WJCC*, Vol. 3, No. 1, pp. 52-57, (2015).

[5] J. G. Lee, *Computational materials science an introduction*, 2nd ed., CRC Press, New York, (2016).

[6] Z. D. Sha, W. H. Wong, Q. Pei, P. S. Branicio, L. Zishun, T. Wang, T. Guo adn H. Gao, "Atomistic origin of size effects in fatigue behavior of metallic glasses", *J Mech Phys Solids.*, Vol. 104, No. 7, pp. 84-95, (2017).

[7] M. R. Akbarpour, H. M. Mirabad, A. Hemmati and H. S. Kim, "Processing and microstructure of Ti-Cu binary alloys: A comprehensive review", *Prog. Mater. Sci.*, Vol. 127, No. 6, pp. 3306, (2022).

[8] L. Verlet, "Computer experiment on classical fluids, I. Thermodynamical properties of lennard-jones molecules", *Phys. Rev.*, Vol. 159, No. 1, pp. 98-103, (1967).

[9] G. C. Ma, J. L. Fan and H. R. Gong, "Mechanical behavior of Cu-W interface systems upon tensile loading from molecular dynamics simulations", *Comput. Mater. Sci.*, Vol. 152, No. 9, pp. 165-168, (2018).

[10] W. M. Choi, Y. Kim, D. Seol and B. J. Lee, "Modified embedded-atom method interatomic potentials for the Co-Cr, Co-Fe, Co-Mn, Cr-Mn and Mn-Ni binary systems", *Comput. Mater. Sci.*, Vol. 130, No. 4, pp. 121-129, (2017).

[11] M. Luo, L. Liang, L. Lang, S. Xiao, W. Hu and H. Deng, "Molecular dynamics simulations of the characteristics of Mo/Ti interfaces", *Comput. Mater. Sci.*, Vol. 141, No. 1, pp. 293-301, (2018).

[12] G. J. Ackland, M. I. Mendelev and T. L. Underwood, "Development of an interatomic potential for the simulation of defects, plasticity and phase transformations in titanium", *J. Chem. Phys.*, Vol. 145, No. 10, pp. 1-33, (2016).

[13] V. Fotopoulos, C. S. O'Hern, M. D. Shattuck and A. L. Shluger, "Modeling the effects of varying the Ti concentration on the mechanical properties of Cu-Ti alloys", *ACS Omega*., Vol. 9, No. 9, pp. 10286-10298, (2024).

[14] D. N. Trong, V. C. Long and S. Ţălu, "Molecular dynamics simulation of bulk Cu material under various factors", *Appl. Sci.*, Vol. 12, No. 9, pp. 4437, (2022).

[15] T. T. Quoc, V. C. Long, S. Ţălu and D. N. Trong, "Molecular Dynamics Study on the Crystallization Process of Cubic Cu–Au Alloy", *Appl. Sci.*, Vol. 12, No. 1, pp. 946, (2022).

[16] A. A. Kharisma, H. Rudianto, A. B. Mutiara, S. Puspitodjati, F.H. Latief, W. A. Sukarto, W.B. Widyatno, D. Aryanto and C. Firdharini, "The effects of copper on the mechanical properties of Ti-10Mo alloy prepared by powder metallurgy method", *J Met Mater Miner*., Vol. 34, No. 1, pp. 1813, (2024).

[17] D. N. Trong, V. C. Long, U. Saraç, V. D. Quoc and S. Ţălu, "First-principles calculations of crystallographic and electronic structural properties of Au-Cu alloys", *J. Compos. Sci.*, Vol. 6, No. 12, pp. 383-394, (2022).

[18] T. T. Quoc, P. N. Dang, D. N. Trong, V. C. Long and Ş. Ţălu, "Molecular dynamics study influence of factors on the structure, phase transition, and crystallization of the $Ag_{1-x}Au_x$, x = 0.25, 0.5, 0.75 alloy", *Mater. Today Commun.*, Vol. 37, No. 2, pp. 107119, (2023).

[19] D. N. Trong, V. C. Long and S. Ţălu, "The structure and crystallizing process of NiAu alloy: a molecular dynamics simulation method", *J. Compos. Sci.*, Vol. 5, No. 1, pp. 18-32, (2021).

[20] D. N. Trong, V. C. Long and S. Ţălu, "Effects of number of atoms and doping concentration on the structure, phase transition, and crystallization process of $Fe_{1-x-y}Ni_xCo_y$ alloy: A molecular dynamic study", *Appl. Sci.*, Vol. 12, No. 17, pp. 8473, (2022).

[21] O. Ashkani, M. R. Tavighi, M. Karamimoghadam, M. Moradi, M. Bodaghi and M. Rezayat, "Influence of aluminum and copper on mechanical properties of biocompatible Ti-Mo alloys: A simulation-based investigation", *Micromachines.*, Vol. 14. No. 5, pp. 1081-1094, (2023).

[22] Z. Gao, H. Luo, Q. Li and Y. Wan, "Preparation and characterization of Ti-10Mo alloy by mechanical alloying," *Metallogr. Microstruct. Anal.*, Vol. 1, pp. 282-289, (2012).

[23] R. Arifin, F. Astuti, M. A. Baqiya, Y. Winardi, Y. A. Wicaksono, Darminto and A. Selamat, "Structural change of TiAl alloy under uniaxial tension and compression in the <001> direction : A molecular dynamics study", *MDPI: Metals.*, Vol. 11, No. 11, pp. 1-14, (2021).

[24] R. Arifin, D. R. P. Setiawan, D. Triawan, A. F. S. Putra, Munaji, Y. Winardi, W. T. Putra and Darminto, "Structural transformation of Ti-based alloys during tensile and compressive loading: An insight from molecular dynamics simulations", *MRS Commun.*, Vol. 13, No. 2, pp. 225-232, (2023).

[25] J. Liu and L. Zhang, "Molecular dynamics simulation of the tensile deformation behavior of the $\gamma(TiAl)/\alpha_2(Ti_3Al)$ interface at different temperatures", *J. Mater. Eng. Perform.*, Vol. 31, No. 2, pp. 918-932, (2022).

[26] H. Ganesan, I. Scheider and C. J. Cryon, "Quantifying the high-temperature separation behavior of lamellar interfaces in γ-titanium aluminide under tensile loading by molecular dynamics", *Comput. Mater. Sci.*, Vol. 7, No. 7 pp. 1-17, (2020).

[27] Z. Li, Y. Gao, S. Zhan, H. Fang and Z. Zhang, "Molecular dynamics study on temperature and strain rate depedences of mechanical properties of single crystal Al under uniaxial loading", *AIP Advances.*, Vol. 10, No. 7, pp. 1-15, (2020).

[28] W. L. Zhou, Y. Liu, B. Y. Wang, Y. Song, C.N. Niu and S. Hu, "Molecular dynamics calculations of stability and phase transformation of TiV alloy under uniaxial tensile test", *Mater. Res. Express.*, Vol. 8. No. 6, pp. 1-13, (2021).

[29] L. Zhao and Y. Liu, "The influence mechanism of the strain rate on the tensile behavior of copper nanowire", *Sci. China Technol. Sci.*, Vol. 62, No. 11, pp. 2014-2019, (2019).

[30] S. C. Tao, J. L. Xu, L. Yuan, J. M. Luo and Y. F. Zheng, "Microstructure, mechanical properties and antibacterial properties of the microwave sintered porous Ti-3Cu alloy," *J. Alloys Compd.*, Vol. 812, No. pp. 152142, (2020).

[31] J. Wang, S. H. Oh and B. J. Lee, "Second-nearest-neighbor modified embedded-atom method interatomic potential for Cu-M (M=Co,Mo) binary systems", *Comput. Mater. Sci.*, Vol. 178, No. 1, pp. 1-6, (2020).

[32] K. Zhou and B. Liu, *Molecular Dynamics Simulation Fundamentals And Applications*, 1st ed., Elsevier, United Kingdom, pp. 5-6, (2022).

[33] S. T. Oyinbo and T.C. Jen, "Molecular dynamics investigation of temperature effect and surface configurations on multiple impacts plastic deformation in a palladium-copper composite metal membrane (CMM): A cold gas dynamic spray (CGDS) process", *Comput. Mater. Sci.*, Vol. 185, pp. 109968, (2020).

[34] K. Nordlund, *Introduction to molecular dynamics*, University of Helsinki, Finland, pp. 65, (2015).

[35] Plimpton and J. Steven, "*LAMMPS and classical molecular dynamics for materials modeling". Conference: Proposed for presentation at the OLCF",* United States, pp. 6-12, (2015).

[36] S. Nose, "A molecular dynamics method for simulations in the canonical ensemble", *Mol. Phys.*, Vol. 52, No. 2, pp. 255-268, (1984).

[37] W. G. Hoover, "Canonical dynamics: Equilibrium phase-space distributions", *Phys. Rev. A.*, Vol. 31, No. 3, pp. 1695-1697, (1985).

[38] M. A. Tschopp, D. E. Spearot and D. L. McDowell, "Atomistic simulations of homogeneous dislocation nucleation in single crystal copper", *Model. Simul. Mater. Sci. Eng.*, Vol. 15, No. 7, pp. 693-710, (2007).

[39] M. A. Tschopp and D. L. McDowell, "Influence of single crystal orientation on homogeneous dislocation nucleation under uniaxial loading", *J Mech Phys Solids.*, Vol. 56, No. 5, pp. 1806–1830, (2008).

[40] G. J. Ackland and A. P. Jones, "Applications of local crystal structure measures in experiment and simulation", *Phys. Rev. B.*, Vol. 73, No. 5, p. 0541041-054111, (2006).

[41] C. L. Kelchner, S. J. Plimpton and J. C. Hamilton, "Dislocation nucleation and defect structure during surface indentation", *Phys. Rev. B.*, Vol. 58, No. 17, pp. 11085-11088, (1998).

[42] J. Wang, Z. Ren, S. Yang, J. Ning, S. Zhang and Y. Bian, "The influence of the strain rate and prestatic stress on the dynamic mechanical properties of sandstone- A case study from china", *Materials.*, Vol. 16, No. 9, pp. 3591-3605, (2023).

[43] N. Abbasnezhad, A. Khavandi, J. Fitoussi, H. Arabi, M. Shirinbayan and A. Tcharkhtchi, "Influence of loading conditions on the overall mechanical behavior of polyether-ether-ketone (PEEK)", *Int. J. Fatigue.*, Vol. 109, No. 4, pp. 83-92, (2018).

[44] X. Mao, A. Shi, R. Wang, J. Nie, G. Qin, D. Chen and E. Zhang, "The influence of copper content on the elastic modulus

How to cite this paper:

Aji Abdillah Kharisma, Haris Rudianto, Achmad Benny Mutiara and Sulistyo Puspitodjati, "The effect of Cu concentration on tensile and compression properties of Ti-10Mo alloy using molecular dynamics simulations,", *J. Comput. Appl. Res. Mech. Eng.*, Vol. 14, No. 1, pp. 129-141, (2024).

DOI: 10.22061/jcarme.2024.10461.2377

URL: https://jcarme.sru.ac.ir/?_action=showPDF&article=2201